Determination of Lithium-Ion Distributions in Nanostructured Block Polymer Electrolyte Thin Films by X-ray Photoelectron Spectroscopy Depth Profiling

Jonathan B. Gilbert,[†] Ming Luo,[‡] Cameron K. Shelton,[‡] Michael F. Rubner,[*,§] Robert E. Cohen,[*,†] and Thomas H. Epps, III[*,‡]

[†]Department of Chemical Engineering, Massachusetts Institute of Technology, Cambridge, Massachusetts 02139, United States, [‡]Department of Chemical and Biomolecular Engineering, University of Delaware, Newark, Delaware 19716, United States, and [§]Department of Materials Science and Engineering, Massachusetts Institute of Technology, Cambridge, Massachusetts 02139, United States. J.B.G. and M.L. contributed equally to this work.

ABSTRACT X-ray photoelectron spectroscopy (XPS) depth profiling with C_{60}^+ sputtering was used to resolve the lithium-ion distribution in the nanometer-scale domain structures of block polymer electrolyte thin films. The electrolytes of interest are mixtures of lithium trifluoromethanesulfonate and lamellar-forming polystyrene–poly(oligo(oxyethylene)methacrylate) (PS–POEM) copolymer. XPS depth profiling results showed that the lithium-ion concentration was directly correlated with the POEM concentration. Furthermore, chemical state and atomic composition of the film were analyzed through the deconvolution of the C1s signal, indicating that the lithium ions appear to be uniformly distributed in the POEM domains. Overall, the unique capabilities of C_{60}^+ depth profiling XPS provide a powerful tool for the analysis of nanostructured polymer thin films in applications ranging from energy storage and generation to surface coatings and nanoscale templates.

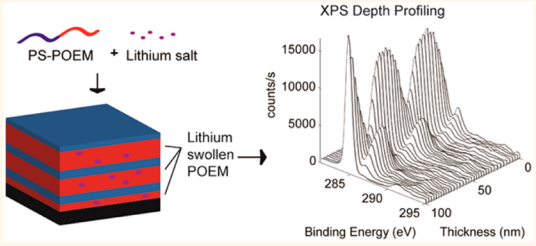

KEYWORDS: block polymer · electrolyte · salt-doping · thin film · ion distribution · XPS depth profiling · C_{60}^+

Block polymer thin films provide a platform for the creation of a variety of nanostructured soft materials for applications ranging from drug delivery,[1] to membranes,[2] to nanolithography,[3] to electronic materials.[4] In recent years, block polymers with an ion-solvating block, typically poly(ethylene oxide) (PEO), and a nonconducting block such as polystyrene (PS), have received considerable attention as viable rechargeable battery membrane materials because of their high thermal, mechanical, and electrochemical stabilities compared to the traditional liquid or gel-like electrolyte systems.[5] The liquid-like PEO block (usually complexed with a metal salt such as a lithium salt) forms ion-conducting pathways, while the rigid PS block provides mechanical strength to resist lithium dendrite formation and confer thermal and mechanical stability. Because the conductivity and mechanical strength are decoupled, it becomes possible to design battery systems that simultaneously address improvements in ion conductivity and mechanical properties.[6,7]

Extensive studies have focused on elucidating the relationship between mechanical properties, ionic conductivity, and block polymer morphologies.[5,8–12] While the morphology effects on mechanical properties of block polymer electrolytes have been well-studied and understood,[11,12] the morphology effects (domain structure, domain size, *etc.*) on the ionic conductivities are much more complicated. In the simplest symmetric PS–PEO lamellar systems doped with lithium salt, Panday *et al.* demonstrated that the ion conductivity increased with increasing molecular weight of the PEO

* Address correspondence to rubner@mit.edu, recohen@mit.edu, thepps@udel.edu.

Received for review October 8, 2014 and accepted December 19, 2014.

Published online December 19, 2014
10.1021/nn505744r

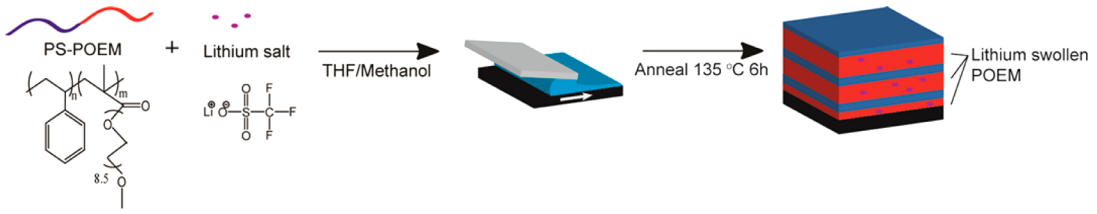

Figure 1. Fabrication schematic of lamellar PS−POEM lithium-doped thin films.

block (M_{PEO}, 7−98 kg/mol),[7] while Yuan *et al.* investigated the low molecular regime (M_{PEO}, 1.5−7 kg/mol) and found that the ion conductivity decreased with increasing M_{PEO}.[13] This non-monotonic change in the conductivity of the block polymer systems with changing molecular weight (changing lamellar domain size) prompted efforts to understand the influence of local ion distribution in lamellar domains on conductivity. Gomez *et al.* presented the first direct imaging of lithium ions in a PS−PEO bulk system using energy-filtered transmission electron microscopy (EFTEM).[14] They showed that the lithium salt was progressively more localized to the middle of the PEO lamellae with increasing M_{PEO} (16−98 kg/mol), and the increase of ion conductivity at higher molecular weights was strongly correlated to the localization of the lithium cation. The authors attributed the localization effect to inhomogeneous local stress field in block polymer microdomains, as calculated from self-consistent field theory for the salt-free system. However, the quantitative determination of salt distribution profiles was difficult by EFTEM. Additionally, in contrast to that report, a uniform distribution of lithium ions was posited by Nakamura and Wang when accounting for the salt effect, suggesting that factors such as electrostatic potential and local solvation energy are equally important in affecting the ion distribution.[15]

To address this unresolved and important topic, we employed X-ray photoelectron spectroscopy (XPS) depth profiling with C_{60}^+ sputtering to determine the ion distribution in lithium salt-doped block polymer thin films. Single-ion sputtering sources like Ar^+ or Cs^+ cause severe damage to soft materials that can alter the chemical composition and confound analysis.[16,17] In contrast, cluster-ion sputtering sources like C_{60}^+ result in much less damage, as the energy transfer from the ion to the material occurs primarily at the film surface, minimizing the propagation of damage into the depth of the film.[18] This method recently showed its effectiveness in measuring interlayer diffusion and material exchange in nanostructured polyelectrolyte multilayer films.[19]

The electrolytes of interest are mixtures of lithium trifluoromethanesulfonate (lithium triflate) and lamellar-forming PS−poly(oligo(oxyethylene)methacrylate) (PS−POEM) copolymer. Although the room temperature conductivity of this PEO-grafted block polymer is of great interest given the substantial improvement over a PEO−linear block polymer,[20,21] the lithium-ion distribution in the POEM domain has not been explored. Through XPS depth profiling analysis, we confirmed the presence of the lithium salt in the POEM region and found that the lithium distribution was directly correlated to the POEM concentration. Furthermore, we found that depth profiling XPS with C_{60}^+ sputtering has the potential to analyze the nanostructure in a variety of soft materials systems.

RESULTS AND DISCUSSION

The PS−POEM used in this study had an overall molecular weight of 36 kg/mol (PS_{20k}−$POEM_{16k}$) and formed lamellae in the bulk with domain spacing (L_0) of 26.1 nm [determined from small-angle X-ray scattering (SAXS); see Supporting Information]. Thin films of PS−POEM doped with lithium triflate were fabricated as illustrated in Figure 1, and uniform thickness and gradient thickness films (80−130 nm) were flow-coated[22] from a blend solution onto toluene-rinsed and ultraviolet-ozone (UVO)-treated silicon wafers. The salt concentration (ether oxygen to lithium cation ratio, [EO]:[Li]) was either 12:1 or 6:1. After casting, the thin films were annealed at 135 °C under vacuum for 6 h to promote the formation of parallel-oriented lamellar nanostructures in the films, which was ideal for the intradomain characterization of the thin films by XPS.

Nanostructured Block Polymer Electrolyte Films. The domain structure of the thin film samples were characterized by optical microscopy and atomic force microscopy (AFM). The optical images revealed that the gradient thickness films exhibited cyclic changes between island/hole structures and uniform surface regions (Figure 2a), which was expected for parallel orientations of lamellar nanostructures in thin film geometries.[23] The lamellar domain spacing was determined from the height of the island/hole structures through AFM. Upon salt loading, the lamellar domain spacing (L_0) increased from 26.8 nm (neat) to 36.0 nm (12:1 [EO]:[Li]) to 41.3 nm (6:1 [EO]:[Li]) (Figure 2b), as the salt preferentially swelled the POEM domain.[14] This increase in domain spacing was consistent with SAXS measurements of the comparable bulk materials (Figure 2c). The substantial change in domain spacing (over 50%) without a phase transition has been reported in other salt-doped block polymer systems.[24] From commensurability calculations, the PS−POEM films showed prominent island/hole structures at film thicknesses of nL_0 and uniform

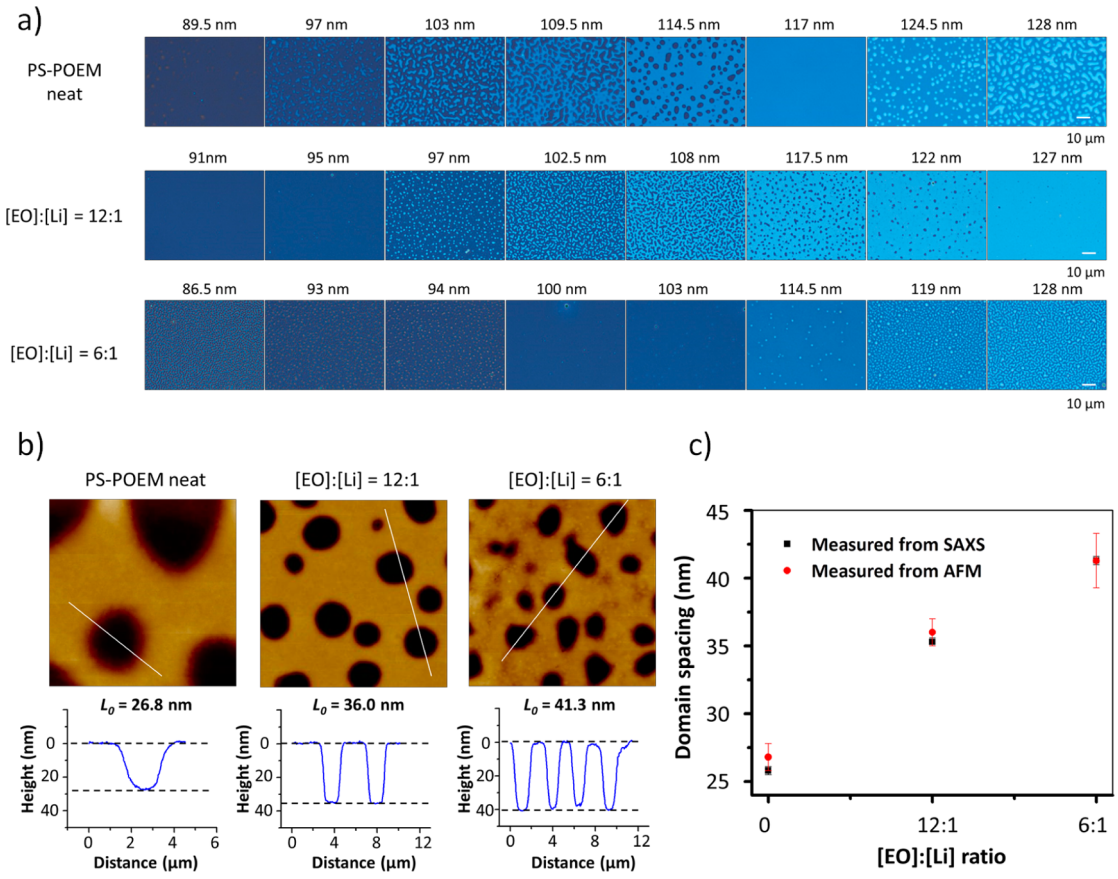

Figure 2. (a) Optical images of gradient thickness PS−POEM films (neat, [EO]:[Li] = 12:1 and 6:1) annealed at 135 °C for 6 h. (b) AFM height images and corresponding sections showed that the difference between the high and low regions are L_0. (c) Comparison of the measured domain thickness between AFM and SAXS.

surfaces at $(n + 0.5)L_0$, which indicated an asymmetric wetting conditions.[23] Due to the affinity of the polar methacrylate-based backbone and PEO side chain for the hydrophilic silicon oxide surface, the POEM block tended to segregate to the substrate. The PS block resided at the free surface, supporting an asymmetric wetting assignment (the presence of POEM at the substrate and PS at the top surface was confirmed by XPS as discussed in a later section).

We also conducted X-ray reflectivity (XRR) experiments on the thin film samples ([EO]:[Li] = 12:1 and 6:1) to confirm the layered structures. The film thicknesses were ∼90 nm for the [EO]:[Li] = 12:1 sample and ∼102 nm for the [EO]:[Li] = 6:1 sample; thus, both of the films were at commensurate film thickness ($5L_0/2$). Figure 3 shows the measured and model calculated XRR profiles for these two samples. The thin film model for the calculated profile incorporates a capping layer of PS at the air surface, a wetting layer of POEM at the substrate, and two repeats of POEM and PS layers in the bulk of the film. Because it is well-known that salt solutions do not obey the ideal mixing rule,[25] the density of the salt-doped POEM layer was estimated from separate measurements on a salt-doped POEM homopolymer film ([EO]:[Li] = 6:1) using XRR; the density of the PS layer was based on values from the literature.[26] We found that the lamellar repeats (consisting of a POEM layer and a PS layer) were ∼36 nm for the [EO]:[Li] = 12:1 sample and ∼40 nm for the [EO]:[Li] = 6:1 sample, respectively. These values were in good agreement with the domain spacings measured from AFM and SAXS. Additionally, the fitted PS layer thickness was approximately 16 nm, which was similar to the values in the neat PS−POEM.

The interface roughness (interfacial mixing) from the XRR model further was compared to the interfacial width calculated from self-consistent field theory. The segregation strength χN (χ is the segment−segment Flory−Huggins interaction parameter, and N is the total degree of polymerization) for the neat PS−POEM was ∼50 at 135 °C, and the interfacial width was estimated to be ∼2 nm (calculations are in the Supporting Information). Previous theoretical and experimental work suggests an increase in χ upon salt doping;[15,21,25,27,28] therefore, we expect that the blocks become less compatible, and the interfacial width should decrease with increasing salt concentration. However, complications can arise when adding salt. For example, the salt may induce mixing in diblock copolymers as recently found by Teran *et al.*[25] In this work, we employ XRR as a simple but reasonably accurate method for the estimation of interfacial

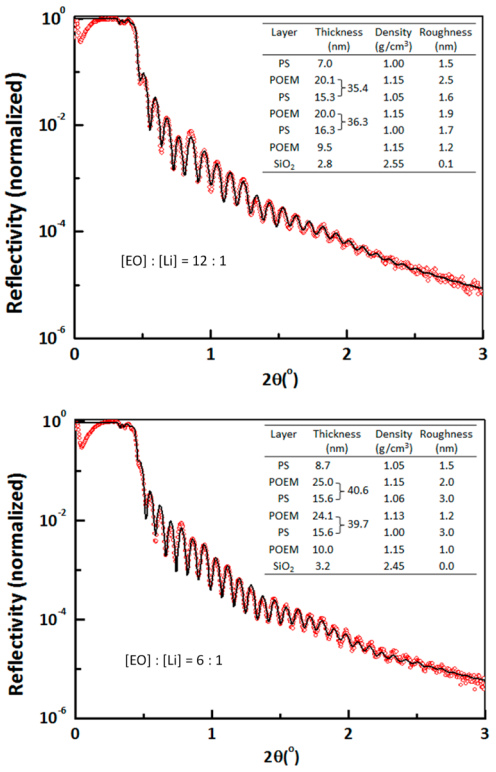

Figure 3. X-ray reflectivity profile for lithium-doped PS−POEM films with [EO]:[Li] of 12:1 (top) or 6:1 (bottom). The red "o" symbols denote the measured profile, and the solid line denotes the fit profile. The inset tables list the fitting parameters for the model for which the "Roughness" corresponds to the likely interfacial width between layers.

mixing within block polymer electrolytes. The interface roughness was ~1.8 ± 0.5 nm for the [EO]:[Li] = 12:1 sample and ~2.0 ± 0.5 nm for the [EO]:[Li] = 6:1 sample. Hence, this study was not able to resolve a change in the interfacial width at greater salt loadings, which may suggest a more detailed study on interfacial mixing in block polymer electrolyte systems in the future.

XPS Depth Profiling with C_{60}^+ Cluster-Ion Sputtering. To resolve the material distribution profile normal to the substrate in the oriented lamellar film, C_{60}^+ cluster-ion depth profiling XPS was used. The alternative EFTEM technique is less quantitative for thin film analysis of dopants, such as lithium, due to their small concentrations across the domains, and sample preparation and image analysis can be tedious depending on the nanostructure orientation. We note that the choice of EFTEM *versus* cluster-ion XPS can be system- (or nanostructure-) dependent,[29,30] as each technique has potential limitations. XPS depth profiling is suitable for lamellar-forming block polymers and also may be useful for probing domain profiles in other self-assembled nanostructures.[31,32] Using iterative etching and XPS data collection (Figure 4a), the discrete nanostructured lamellar regions noted in the XRR results could be reproduced. To minimize X-ray damage, a large sample area (~0.1 mm^2) was analyzed. Furthermore, film thicknesses were chosen such that the film was free of island/hole structures (film thickness = 117 nm, $4.5L_0$ for neat PS−POEM film; film thickness = 102 nm, $2.5L_0$ for PS−POEM with [EO]:[Li] = 6:1). Figure 4b shows the alternating C1s and O1s signal of the neat lamellar thin film. Near the silicon substrate, a significant signal from the Si2p peak was identified as well as an increase in the O1s signal due to SiO_2. Figure 4c displays the alternating intensity of the O1s spectra for which the red spectra represent the POEM layers (high oxygen content in EO side chains) and the blue spectra correspond to the PS layers (very low, but nonzero oxygen content owing to etching roughness effects[33]). The C1s signal in Figure 4d depicts a similar alternating structure, and two C1s peaks (285.0 and 286.5 eV) could be detected. For the blue spectra representing the PS layers, the C1s peak at 285.0 eV corresponds to carbon−carbon bonds and is the dominant feature. For the red spectra representing the POEM layers, the C1s peak at 286.5 eV primarily results from the ether bonds in the PEO side chain. There was also a carbon−carbon bonding peak in the red spectra at 285.0 eV due to the carbon−carbon backbone with a minor contribution from the underlying PS layer. The atomic profile in Figure 4c,d also supports the notion that the film demonstrates asymmetric wetting, with PS at the air interface and POEM in contact with the substrate.

Determination of Lithium-Ion Distribution. To analyze the distribution of lithium ions within block polymer electrolyte films, the effective C_{60}^+ etch rate was decreased to allow for higher resolution in the axial distribution. Also, lithium salt was added at a [EO]:[Li] = 6:1 ratio to maximize the lithium signal. Figure 5d−g shows the alternating C1s, Li1s, F1s, and O1s signals and the resulting depth profile (Figure 5a) captured the repeating structure of a lamellar PS−POEM film doped with lithium salt. The domain spacing as measured by the distance between the peaks of Figure 5a (~40 nm) also matched the spacing measured *via* XRR (Figure 3). Furthermore, in the O1s-rich region, there was significant Li1s and F1s signal, supporting the segregation of the lithium ion and fluorine-containing triflate counterion ($CF_3SO_3^-$) in the oxygen-rich POEM layers. This capability to measure accurate domain structure and atomic composition as a function of depth in organic nanostructured films is a strength of cluster-ion depth profiling XPS.

The sinusoidal nature of the atomic concentration profile in Figure 5a has been seen previously in nanostructured inorganic multilayer systems analyzed with secondary ion mass spectrometry (SIMS) and depth profiling XPS.[33,34] The broadened interface can be attributed to experimental effects such as etching-induced roughness (σ), atomic mixing (w), and the inelastic mean free path (IMFP) (λ) of the photoelectron measured. To enable the analysis of the underlying

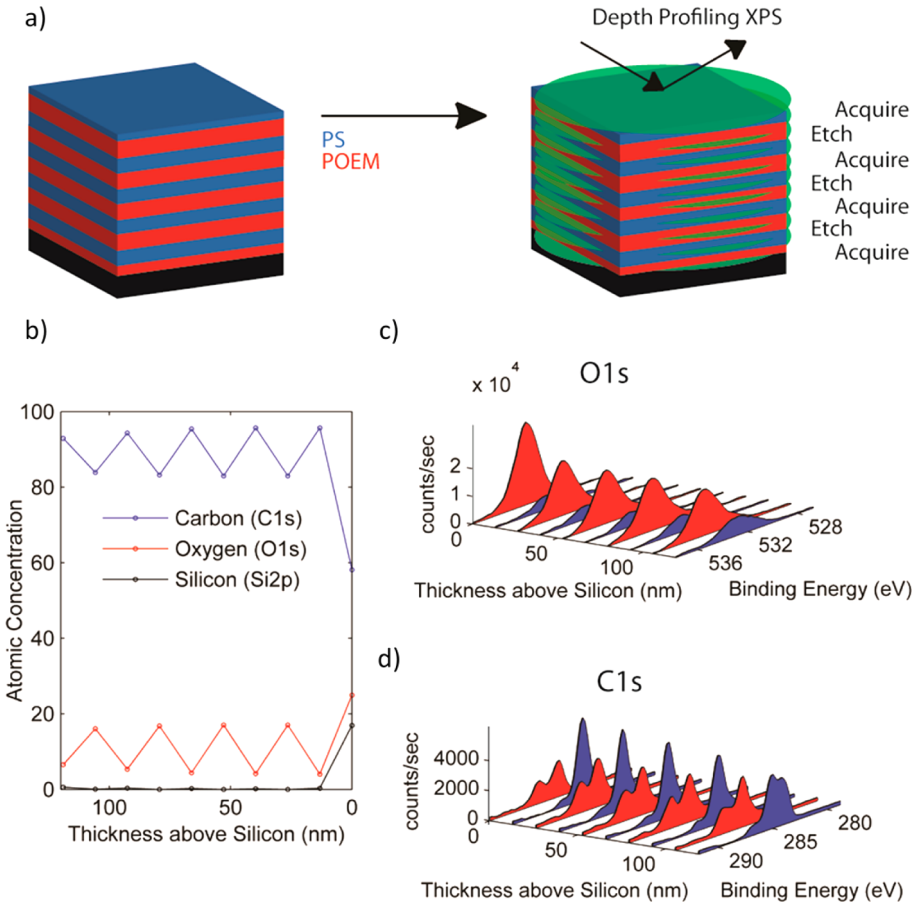

Figure 4. Depth profiling XPS of 36 kDa PS–POEM without lithium salt. (a) Schematic of depth profiling XPS analysis. (b) Atomic concentration *versus* thickness above the silicon substrate. (c,d) O1s and C1s photoelectron spectra, respectively, showing the alternating intensity of a lamellar block polymer film. The red and blue spectra are primarily representative of the POEM and PS lamellae, respectively.

structure, Hofmann *et al.* developed an analytical technique called the mixing-roughness-information depth (MRI) model to account for these effects.[35] The MRI model showed excellent agreement with the depth profiling XPS data when σ = 5 nm was used (Figure 6). Because roughness likely is a dominant factor altering the profile, studies should consider employing the lowest beam energy possible, along with sample rotation and a large incidence angle to achieve the best resolution.

To determine the pairing or dissociation state of the lithium ion and the fluorine-containing counterion, the F1s signal was multiplied by the molar ratio of lithium to fluorine in the lithium salt (1:3) (see Figure 5b). The resulting profile, "F1s:Li1s scaled", allows for direct comparison of atomic concentrations. As "F1s:Li1s scaled" overlays very closely with the Li1s signal, it indicates that the lithium ion and the fluorine-containing triflate anion have a similar distribution in the POEM domains.[14]

The local distribution of lithium ion within the POEM lamellae could be determined by further analyzing the atomic and chemical composition of the film, as demonstrated in Figure 5c. In the salt-doped PS–POEM system, there are only two sources of oxygen (POEM and the lithium salt); by subtracting the contribution of the triflate counterion from the total oxygen signal, the axial distribution of the POEM within the film could be determined. Because the counterion ($CF_3SO_3^-$) has an equal molar ratio of fluorine and oxygen, the F1s signal represents the distribution of the triflate counterion. Therefore, the POEM concentration ("POEM from O1s") was determined by subtracting the F1s concentration from the O1s concentration. A complementary method for analyzing the POEM distribution is through component analysis of the C1s region. As shown in Figure 5d, the C1s region contained a variety of peaks, each corresponding to different chemical bonding states present within the block polymer. For example, the alternating photoelectron peaks found at 285.0 and 286.5 eV are related to carbon–carbon bonds in the PS region and ether bonds in the POEM region, respectively. Using the known binding energy of the polymer components, the C1s peaks could be deconvoluted and directly assigned to lithium salt (CF_3), PS, or POEM. An example of fitting the spectra with these peaks in both a PS-rich region and a POEM-rich region is provided in Figure S1.

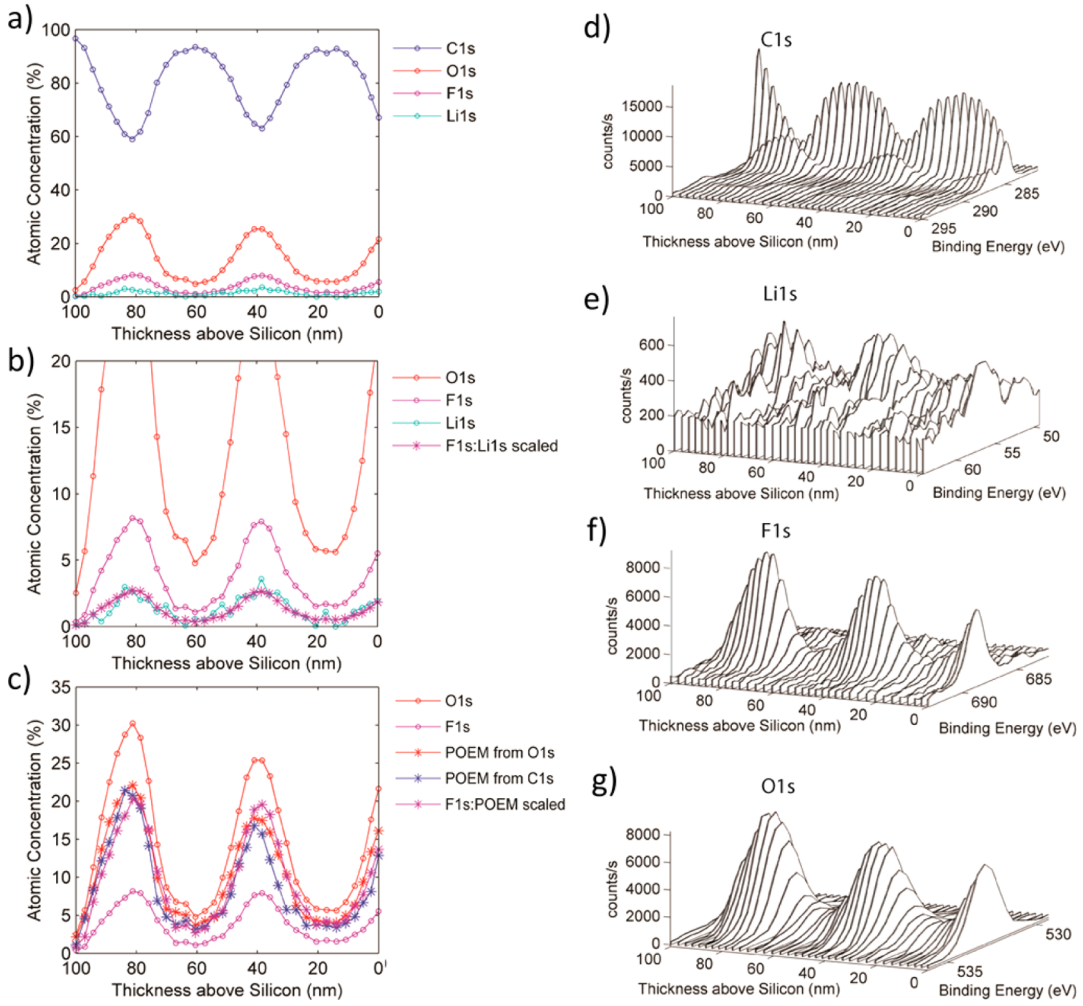

Figure 5. XPS depth profiling of PS−POEM doped with Li salt ([EO]:[Li] = 6:1). (a) Atomic concentration profile with depth. (b) Rescaled atomic concentration profile with depth to focus on lower concentration species, including overlay of F1s scaled to Li1s signal. (c) Distribution of POEM block within the film analyzed *via* O1s signal or fitting the C1s peaks. To compare the salt distribution to the POEM distribution, the F1s is scaled to POEM. (d−g) Three-dimensional spectra of the C1s, Li1s, F1s, and O1s regions, respectively. The differing etch rates of PS *versus* POEM (see Supporting Information Table S2) were considered in plotting the data.

The corresponding POEM distribution from the C1s component analysis is plotted in Figure 5c ("POEM from C1s"), and the results of the two methods ("POEM from O1s" and "POEM from C1s") were qualitatively similar. It is important to note that the capability to analyze the chemical composition as well as the atomic concentration is not easily possible using other analysis techniques such as SIMS or EFTEM.

A final step in the analysis was to determine the distribution of the lithium salt within the POEM layers. To enable a direct comparison between the lithium salt and the POEM on the same scale, the F1s concentration was multiplied by its molar ratio within the POEM region. F1s was used in place of the Li1s signal because the F1s signal had a higher signal-to-noise ratio, and earlier analysis showed that the F1s and Li1s concentrations are tightly correlated (Figure 5b). The scaling of the lithium salt distribution was accomplished by multiplying the F1s concentration by the molar ratio of oxygen in the block polymer to fluorine in the salt (10.5:4.25 in [EO]:[Li] = 6:1 salt films; see Table S1). The similarity of the "F1s:POEM scaled" profile to the POEM profile suggests that the lithium salt concentration directly correlates with the POEM concentration. If the lithium concentration was nonuniformly distributed, one would not expect to see the coupling of the POEM and "F1s:POEM scaled" distributions as shown in Figure 5c.

CONCLUSIONS

In summary, we quantitatively determined the distribution of lithium salt within the nanoscale domains of a block polymer electrolyte thin film, which has critical implications for understanding the interplay between salt distribution and ionic conductivity in nanostructured systems. More specifically, we demonstrated that the concentrations of lithium ion and the fluorine-containing triflate anion were tightly correlated,

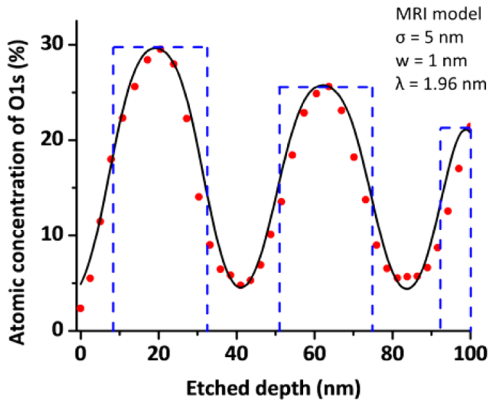

Figure 6. MRI model fit for the measured O1s depth profile. The dot symbols denote the measured profile, and the solid line denotes the fit profile from the MRI model. The dashed lines represent the position of the POEM block according to XRR results. Etching roughness (σ) and atomic mixing (w) were determined from the best fit to the depth profile. The information depth (λ) was estimated using the inelastic mean free path (IMFP) of O1s. Decreasing POEM intensity is noted due to X-ray damage and etching roughness.

and the lithium ion appeared to be uniformly distributed in the POEM (side chain oligoethylene oxide) domains of lamellar PS–POEM films. These results differ from a previous investigation of ion distributions in (main chain ethylene oxide) block polymers (PEO) gleaned from electron microscopy;[14] however, the apparent discrepancies could be explained by the intricacies of the copolymer architectures, with differences in energetics resulting from the coordination of metal ions to side chain *versus* main chain solubilizing segments.[36] Our findings provide the first support for a recent theoretical work predicting uniform lithium-ion distributions in which the lithium ions are assumed to freely distribute among the binding sites of the different PEO chains, subject to the electrostatic interaction with the cations and the solvation energy.[15] We believe that the side chains of POEM have higher chain mobility and increase the freedom to coordinate lithium ions, leading to a more uniform distribution of lithium ions across POEM domains. Thus, our work highlights the need for continued and detailed investigations into the localization of blended constituents with self-assembling macromolecular systems. Finally, this effort was enabled by cluster-ion depth profiling XPS, which facilitated the analysis of both chemical and atomic information as a function of depth. The unique capabilities of C_{60}^+ depth profiling XPS as demonstrated herein are potentially applicable to investigations of nanoscale distributions of molecules in a myriad of polymer thin film systems.

METHODS

Polymer Synthesis. The PS–POEM block polymer was synthesized *via* atom transfer radical polymerization. The PS block was polymerized in a mixture of copper(I) bromide (CuBr), *N*,*N*,*N*′,*N*″,*N*‴-pentamethyldiethylenetriamine and anisole using propargyl 2-bromoisobutyrate as the initiator at 100 °C. The reaction was allowed to proceed for 12 h and terminated by immediate cooling to room temperature and exposure to air. The PS polymer was purified by passage through a neutral alumina column, precipitated from methanol, and dried under dynamic vacuum. To generate the block polymer, the PS was end-capped with bromine[37] and was used as a macroinitiator for chain extension with OEM to generate a PS–POEM block polymer. The final polymer was purified by passage through a neutral alumina column and precipitated in cold isopropyl alcohol. The number-average molecular weight of the PS block (20 000 g/mol) was determined by size exclusion chromatography using PS standards, and the number-average molecular weight of the POEM block (16 000 g/mol) was determined by a combination of ^{1}H NMR spectroscopy and the PS molecular weight. The dispersity of the PS–POEM was 1.18. The calculated weight fraction of the PS block was 0.56. The volume fraction for the PS block was ~0.60 on the basis of polymer densities $\rho_{POEM,25°C}$ = 1.197 g cm^{-3} (measured from densitometer) and $\rho_{PS,25°C}$ = 1.05 g cm^{-3} (from literature[26]); therefore, the PS domain thickness was approximately ~15.6 nm.

Thin Film Preparation. Blends of PS–POEM and $LiCF_3SO_3$ were generated in tetrahydrofuran solution in an Ar glovebox, and methanol was added to the mixture to help dissolve the polymer–salt complex. Uniform thickness and gradient thickness films (80–130 nm) were cast onto toluene-rinsed and UVO-treated silicon wafers using flow coating. Film thickness measurements were obtained using a Filmetrics F20-UV interferometer operated in reflectance mode.

Optical and Atomic Force Microscopy. Optical microscopy images were collected on a Nikon microscope equipped with a 5 MP CCD camera (Nikon Eclipse LV100). The topologies of polymer films were assessed by AFM (Veeco Dimension 3100). Silicon probes (Tap 150G, BudgetSensors) were used in tapping mode. A typical set point ratio was 0.9.

X-ray Reflectivity. XRR was performed for the polymer thin films on an Ultima IV unit (Rigaku). A thin, parallel beam of Cu Kα radiation, λ = 0.154 nm, was incident on the samples. The beam was sized to capture the critical edge of the samples for best results and fit accuracy. XRR profiles were collected by scanning a small incident angle (θ) of X-rays from the source and a detection angle (2θ) of reflected X-rays ($0° < 2\theta < 3°$). The fit profiles across the film thickness were obtained by using Globalfit software.

XPS Depth Profiling with C_{60}^+ Sputtering. Chemical composition of the surface was characterized using a PHI Versaprobe II X-ray photoelectron spectrometer with a scanning monochromated Al source (1486.6 eV, 100 W, spot size 200 μm). Depth profiling was accomplished using the instrument's C_{60}^+ ion source. The takeoff angle between the sample surface and analyzer was 45°, and the X-ray beam collected C1s, O1s, F1s, Li1s, and Si2p elemental information while rastering over a 200 μm × 1400 μm^2 area. Detailed XPS acquisition parameters are in Supporting Information. Sputtering occurred in 1 min intervals, while the sample was moved using concentric Zalar rotation at 1 rpm. The C_{60}^+ source was operated at 10 kV and 10 nA and rastered over a 4 × 4 mm^2 area at an angle 70° to the surface normal. Atomic composition was determined based on photoelectron peak areas, and the relative sensitivity factors were provided in PHI's Multipak processing software. All data were background-subtracted and smoothed using a five-point quadratic Savitzky-Golay algorithm. Data also were charge-corrected so that the carbon–carbon bond has a binding energy of 285.0 eV. No significant increase in temperature occurred (<1 °C) as measured by the temperature of the stage. The surface of the silicon substrate was defined as the point at which the atomic concentration of silicon reached 5% in the depth profiling data. Spectra peaks were fit in CasaXPS, and data were plotted and analyzed using Matlab.

Conflict of Interest: The authors declare no competing financial interest.

Acknowledgment. We acknowledge support by the MRSEC Program of the National Science Foundation (NSF) under award number DMR-0819762. J.B.G. was supported by an NSF and National Defense Science and Engineering Graduate Fellowship. We also acknowledge support from NSF DMR-1207041 to T.H.E., a Martin Luther King, Jr. Visiting Professor Award from MIT to T.H.E., and a DuPont Young Professor Award to T.H.E. We thank Wei-Fan Kuan for synthesizing the PS–POEM polymer. We thank Prof. Michael Mackay and Roddel Remy for assistance with XRR. We also thank the W.M. Keck Electron Microscopy Facility at the University of Delaware for use of their AFM, XRR, and TEM instruments, as well as the help of Libby Shaw at the MIT Center for Material Science and Engineering with XPS. We acknowledge Rosanna Lim for help with spectroscopic ellipsometry.

Supporting Information Available: Additional information, calculation, and figures. This material is available free of charge *via* the Internet at http://pubs.acs.org.

REFERENCES AND NOTES

1. Kelley, E. G.; Albert, J. N. L.; Sullivan, M. O.; Epps, T. H., III. Stimuli-Responsive Copolymer Solution and Surface Assemblies for Biomedical Applications. *Chem. Soc. Rev.* **2013**, *42*, 7057–7071.
2. Yang, S. Y.; Ryu, I.; Kim, H. Y.; Kim, J. K.; Jang, S. K.; Russell, T. P. Nanoporous Membranes with Ultrahigh Selectivity and Flux for the Filtration of Viruses. *Adv. Mater.* **2006**, *18*, 709–712.
3. Maher, M. J.; Bates, C. M.; Blachut, G.; Sirard, S.; Self, J. L.; Carlson, M. C.; Dean, L. M.; Cushen, J. D.; Durand, W. J.; Hayes, C. O.; et al. Interfacial Design for Block Copolymer Thin Films. *Chem. Mater.* **2014**, *26*, 1471–1479.
4. Urbas, A. M.; Maldovan, M.; DeRege, P.; Thomas, E. L. Bicontinuous Cubic Block Copolymer Photonic Crystals. *Adv. Mater.* **2002**, *14*, 1850–1853.
5. Young, W.-S.; Kuan, W.-F.; Epps, T. H., III. Block Copolymer Electrolytes for Rechargeable Lithium Batteries. *J. Polym. Sci., Part B: Polym. Phys.* **2014**, *52*, 1–16.
6. Singh, M.; Odusanya, O.; Wilmes, G. M.; Eitouni, H. B.; Gomez, E. D.; Patel, A. J.; Chen, V. L.; Park, M. J.; Fragouli, P.; Iatrou, H.; et al. Effect of Molecular Weight on the Mechanical and Electrical Properties of Block Copolymer Electrolytes. *Macromolecules* **2007**, *40*, 4578–4585.
7. Panday, A.; Mullin, S.; Gomez, E. D.; Wanakule, N.; Chen, V. L.; Hexemer, A.; Pople, J.; Balsara, N. P. Effect of Molecular Weight and Salt Concentration on Conductivity of Block Copolymer Electrolytes. *Macromolecules* **2009**, *42*, 4632–4637.
8. Majewski, P. W.; Gopinadhan, M.; Osuji, C. O. Understanding Anisotropic Transport in Self-Assembled Membranes and Maximizing Ionic Conductivity by Microstructure Alignment. *Soft Matter* **2013**, *9*, 7106–7116.
9. Weber, R. L.; Ye, Y.; Schmitt, A. L.; Banik, S. M.; Elabd, Y. A.; Mahanthappa, M. K. Effect of Nanoscale Morphology on the Conductivity of Polymerized Ionic Liquid Block Copolymers. *Macromolecules* **2011**, *44*, 5727–5735.
10. Wanakule, N. S.; Panday, A.; Mullin, S. A.; Gann, E.; Hexemer, A.; Balsara, N. P. Ionic Conductivity of Block Copolymer Electrolytes in the Vicinity of Order–Disorder and Order–Order Transitions. *Macromolecules* **2009**, *42*, 5642–5651.
11. Khandpur, A. K.; Foerster, S.; Bates, F. S.; Hamley, I. W.; Ryan, A. J.; Bras, W.; Almdal, K.; Mortensen, K. Polyisoprene–Polystyrene Diblock Copolymer Phase Diagram near the Order–Disorder Transition. *Macromolecules* **1995**, *28*, 8796–8806.
12. Dair, B. J.; Honeker, C. C.; Alward, D. B.; Avgeropoulos, A.; Hadjichristidis, N.; Fetters, L. J.; Capel, M.; Thomas, E. L. Mechanical Properties and Deformation Behavior of the Double Gyroid Phase in Unoriented Thermoplastic Elastomers. *Macromolecules* **1999**, *32*, 8145–8152.
13. Yuan, R.; Teran, A. A.; Gurevitch, I.; Mullin, S. A.; Wanakule, N. S.; Balsara, N. P. Ionic Conductivity of Low Molecular Weight Block Copolymer Electrolytes. *Macromolecules* **2013**, *46*, 914–921.
14. Gomez, E. D.; Panday, A.; Feng, E. H.; Chen, V.; Stone, G. M.; Minor, A. M.; Kisielowski, C.; Downing, K. H.; Borodin, O.; Smith, G. D.; et al. Effect of Ion Distribution on Conductivity of Block Copolymer Electrolytes. *Nano Lett.* **2009**, *9*, 1212–1216.
15. Nakamura, I.; Wang, Z.-G. Salt-Doped Block Copolymers: Ion Distribution, Domain Spacing and Effective χ Parameter. *Soft Matter* **2012**, *8*, 9356–9367.
16. Sanada, N.; Yamamoto, A.; Oiwa, R.; Ohashi, Y. Extremely Low Sputtering Degradation of Polytetrafluoroethylene by C_{60} Ion Beam Applied in XPS Analysis. *Surf. Interface Anal.* **2004**, *36*, 280–282.
17. Tanaka, K.; Sanada, N.; Hikita, M.; Nakamura, T.; Kajiyama, T.; Takahara, A. Surface Depth Analysis for Fluorinated Block Copolymer Films by X-ray Photoelectron Spectroscopy Using C_{60} Cluster Ion Beam. *Appl. Surf. Sci.* **2008**, *254*, 5435–5438.
18. Shard, A. G.; Brewer, P. J.; Green, F. M.; Gilmore, I. S. Measurement of Sputtering Yields and Damage in C_{60} SIMS Depth Profiling of Model Organic Materials. *Surf. Interface Anal.* **2007**, *39*, 294–298.
19. Gilbert, J. B.; Rubner, M. F.; Cohen, R. E. Depth-Profiling X-ray Photoelectron Spectroscopy (XPS) Analysis of Interlayer Diffusion in Polyelectrolyte Multilayers. *Proc. Natl. Acad. Sci. U.S.A.* **2013**, *110*, 6651–6656.
20. Niitani, T.; Shimada, M.; Kawamura, K.; Dokko, K.; Rho, Y.-H.; Kanamura, K. Synthesis of Li^+ Ion Conductive PEO–PSt Block Copolymer Electrolyte with Microphase Separation Structure. *Electrochem. Solid-State Lett.* **2005**, *8*, A385–A388.
21. Ruzette, A.-V. G.; Soo, P. P.; Sadoway, D. R.; Mayes, A. M. Melt-Formable Block Copolymer Electrolytes for Lithium Rechargeable Batteries. *J. Electrochem. Soc.* **2001**, *148*, A537–A543.
22. Stafford, C. M.; Roskov, K. E.; Epps, T. H., III; Fasolka, M. J. Generating Thickness Gradients of Thin Polymer Films *via* Flow Coating. *Rev. Sci. Instrum.* **2006**, *77*, 023908.
23. Albert, J. N. L.; Epps, T. H., III. Self-Assembly of Block Copolymer Thin Films. *Mater. Today* **2010**, *13*, 24–33.
24. Young, W. S.; Albert, J. N. L.; Schantz, A. B.; Epps, T. H., III. Mixed-Salt Effects on the Ionic Conductivity of Lithium-Doped PEO-Containing Block Copolymers. *Macromolecules* **2011**, *44*, 8116–8123.
25. Teran, A. A.; Balsara, N. P. Thermodynamics of Block Copolymers with and without Salt. *J. Phys. Chem. B* **2014**, *118*, 4–17.
26. Momose, A.; Fujii, A.; Kadowaki, H.; Jinnai, H. Three-Dimensional Observation of Polymer Blend by X-ray Phase Tomography. *Macromolecules* **2005**, *38*, 7197–7200.
27. Young, W. S.; Epps, T. H., III. Salt Doping in PEO-Containing Block Copolymers: Counterion and Concentration Effects. *Macromolecules* **2009**, *42*, 2672–2678.
28. Epps, T. H., III; Bailey, T. S.; Waletzko, R.; Bates, F. S. Phase Behavior and Block Sequence Effects in Lithium Perchlorate-Doped Poly(isoprene-*b*-styrene-*b*-ethylene oxide) and Poly(styrene-*b*-isoprene-*b*-ethylene oxide) Triblock Copolymers. *Macromolecules* **2003**, *36*, 2873–2881.
29. Kesava, S. V.; Fei, Z.; Rimshaw, A. D.; Wang, C.; Hexemer, A.; Asbury, J. B.; Heeney, M.; Gomez, E. D. Domain Compositions and Fullerene Aggregation Govern Charge Photogeneration in Polymer/Fullerene Solar Cells. *Adv. Energy Mater.* **2014**, *4*, 1400116.
30. Vajjala Kesava, S.; Dhanker, R.; Kozub, D. R.; Vakhshouri, K.; Choi, U. H.; Colby, R. H.; Wang, C.; Hexemer, A.; Giebink, N. C.; Gomez, E. D. Mesoscopic Structural Length Scales in P3HT/PCBM Mixtures Remain Invariant for Various Processing Conditions. *Chem. Mater.* **2013**, *25*, 2812–2818.
31. Zhao, L. Y.; Eldridge, K. R.; Sukhija, K.; Jalili, H.; Heinig, N. F.; Leung, K. T. Electrodeposition of Iron Core–Shell Nanoparticles on a H-Terminated Si(100) Surface. *Appl. Phys. Lett.* **2006**, *88*, 033111.

32. Sharma, H.; Sharma, S. N.; Singh, S.; Kishore, R.; Singh, G.; Shivaprasad, S. M. Surface Sensitive Probe of the Morphological and Structural Aspects of CdSe Core–Shell Nanoparticles. *Appl. Surf. Sci.* **2007**, *253*, 5325–5333.
33. Wang, J. Y.; Starke, U.; Mittemeijer, E. J. Evaluation of the Depth Resolutions of Auger Electron Spectroscopic, X-ray Photoelectron Spectroscopic and Time-of-Flight Secondary-Ion Mass Spectrometric Sputter Depth Profiling Techniques. *Thin Solid Films* **2009**, *517*, 3402–3407.
34. Hofmann, S. Characterization of Nanolayers by Sputter Depth Profiling. *Appl. Surf. Sci.* **2005**, *241*, 113–121.
35. Hofmann, S. Profile Reconstruction in Sputter Depth Profiling. *Thin Solid Films* **2001**, *398–399*, 336–342.
36. Tarascon, J. M.; Armand, M. Issues and Challenges Facing Rechargeable Lithium Batteries. *Nature* **2001**, *414*, 359–367.
37. Kuan, W.-F.; Roy, R.; Rong, L.; Hsiao, B. S.; Epps, T. H., III. Design and Synthesis of Network-Forming Triblock Copolymers Using Tapered Block Interfaces. *ACS Macro Lett.* **2012**, *1*, 519–523.